First-principles studies of strongly correlated states in defect spin qubits in diamond

He Ma, Nan Sheng, Marco Govoni and Giulia Galli

A Critical Review

Liz Stippell

P.I.: Professor Oleg Prezhdo

Introduction

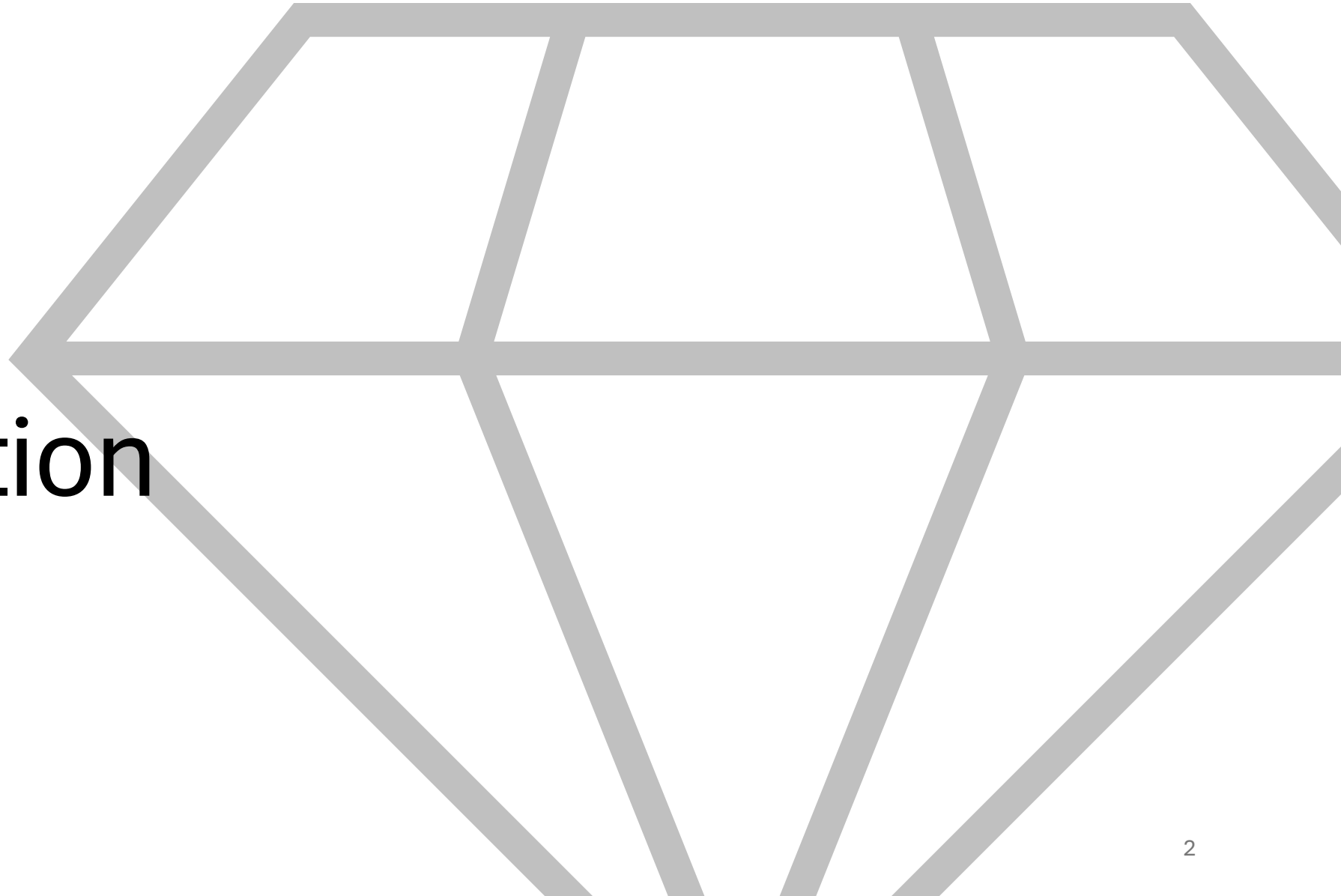

Strongly Correlated Crystalline Systems

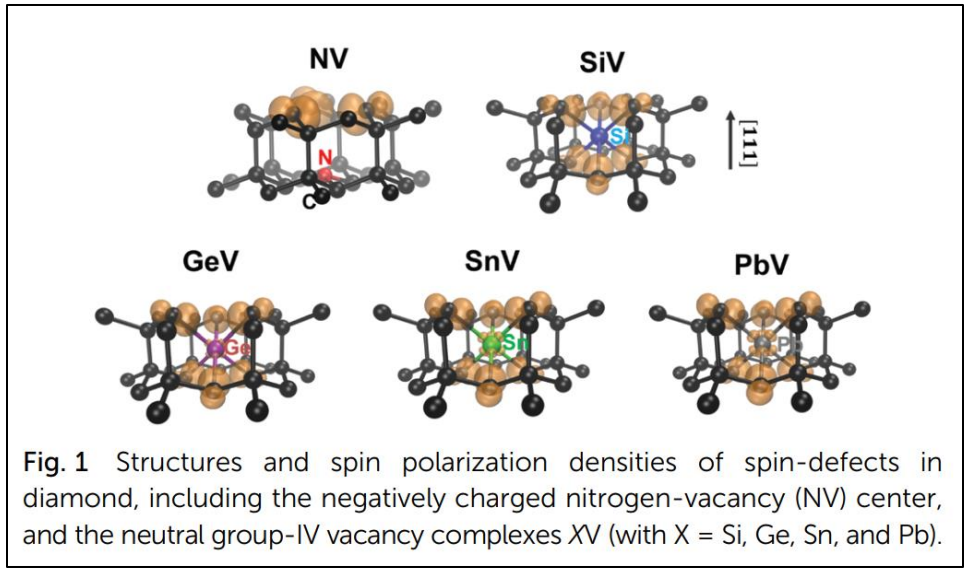

Fig. 1 Structures and spin polarization densities of spin-defects in diamond, including the negatively charged nitrogen-vacancy (NV) center, and the neutral group-IV vacancy complexes *X*V (with X = Si, Ge, Sn, and Pb).

Description

Cannot assume electrons to act independently of one another, needing multireference descriptions of the electrons

Applications

- *Encoding quantum information*
- *Spin defects can illustrate fundamental quantum mechanics principles*
- *Act as quantum sensors*

Multireference Methods

RPA/cRPA

(constrained) Random phase approximation

- Does not account for dielectric screening effects (RPA)
- Effective Hamiltonian describes low-lying excitations using electron-electron interactions

Quantum Embedding

Beyond-RPA

- Accounts for dielectric exchange-correlation effects
- Scalable to systems with hundreds of atoms

REKS-DFT

Spin-restricted ensemble-referenced Kohn-Sham DFT

- Weighted sum of Slater Determinants
- Collapses into KS-DFT for weak correlations

Methods

Theoretical and Computational

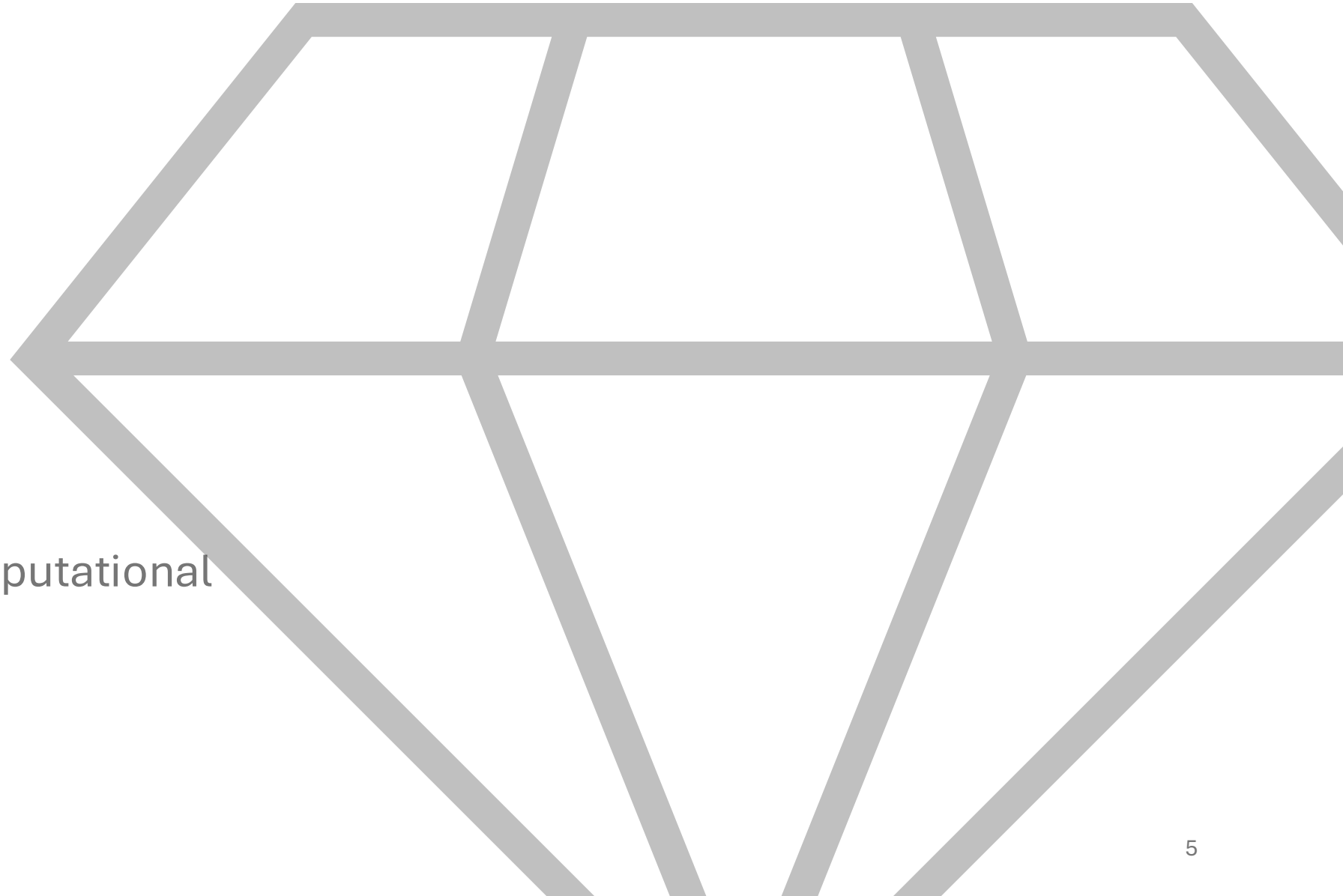

Quantum Embedding Theory

General Theory: The defects are described by a high-level of theory (multireference) whereas the bulk crystal is described by a low-level of theory (single-reference)

Restrict Hamiltonian to active space around Fermi level

$$H = \sum_{ij} t_{ij} a_i^\dagger a_j + \frac{1}{2} \sum_{ijkl} v_{ijkl} a_i^\dagger a_j^\dagger a_l a_k \rightarrow H^{eff} = \sum_{ij} t_{ij}^{eff} a_i^\dagger a_j + \frac{1}{2} \sum_{ijkl} v_{ijkl}^{eff} a_i^\dagger a_j^\dagger a_l a_k$$

t_{ij}

One-electron term
Accounts for kinetic energy and electron-nuclei interaction

v_{ijkl}

Two-electron term
Accounts for Coulomb interaction between electrons

Quantum Embedding Theory: going beyond RPA

RPA/cRPA:

$$v^{eff} = v + \chi^{E}_{rpa} v$$

χ^{E}_{rpa}
Density response function for the environment, E

Quantum Embedding

$$v^{eff} = v + f X^{E} f$$

$$f = v + f_{xc}$$

f_{xc}
Exchange-correlation kernel
Derivative of the exchange-correlation potential w.r.t. the electron density

Computational Workflow

216-atom supercells *(heavy vacancies)*

64-atom supercell *(nitrogen vacancy)*

Ran on quantum computer

Geometry optimization with the PBE functional

Exchange-correlation kernel computed with WEST and Qbox codes

Spin-unrestricted DFT

Obtains ground-state geometries of defects

Spin-restricted DFT

Use ground-state geometries to obtain electronic structure
Creates starting point for the effective Hamiltonian

Quantum embedded calculation

Starting point: PBE

Quantum embedded calculation

Starting point: DDH (dielectric-dependent hybrid)

WEST code

Quantum Espresso

HSE0 functional tested

Information about single-reference calculations:
FCI performed

Results

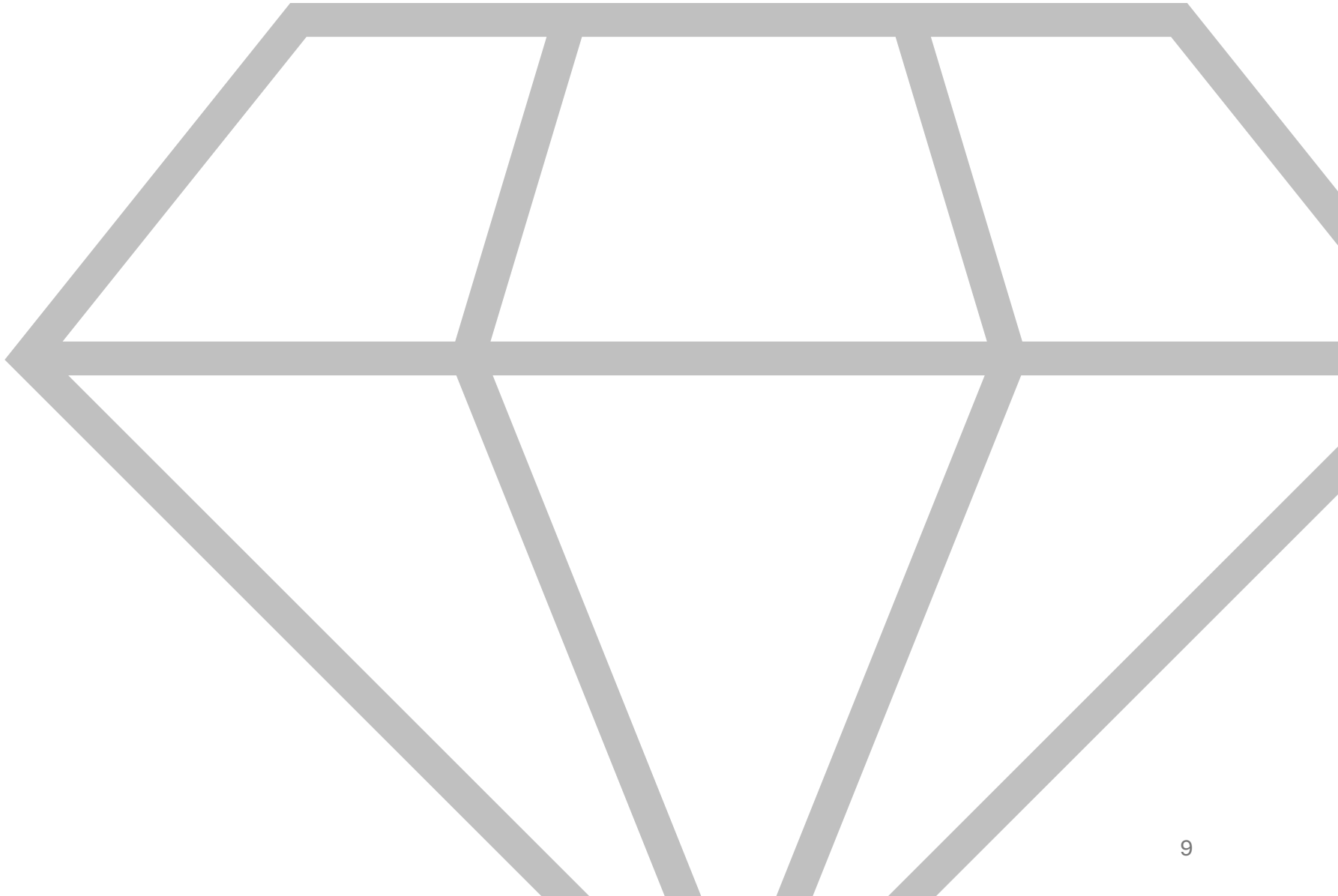

Excitation Energies

System	Excitation	PBE RPA	PBE Beyond-RPA	DDH RPA	DDH Beyond-RPA	Ref.
NV	$^3E \leftrightarrow {}^3A_2$	1.395	1.458	1.921	2.001	2.180[7] (1.945[7])
	$^1A_1 \leftrightarrow {}^3A_2$	1.211	1.437	1.376	1.759	
	$^1E \leftrightarrow {}^3A_2$	0.396	0.444	0.476	0.561	
	$^1A_1 \leftrightarrow {}^1E$	0.815	0.993	0.900	1.198	(1.190[8])
	$^3E \leftrightarrow {}^1A_1$	0.184	0.020	0.545	0.243	(0.344–0.430[12])
SiV	$^3E_u \leftrightarrow {}^3A_{2g}$	1.247	1.258	1.590	1.594	1.568[55] (1.31[54])
	$^3A_{1u} \leftrightarrow {}^3A_{2g}$	1.386	1.416	1.741	1.792	
	$^1E_g \leftrightarrow {}^3A_{2g}$	0.232	0.281	0.261	0.336	
	$^1A_{1g} \leftrightarrow {}^3A_{2g}$	0.404	0.478	0.466	0.583	
	$^1A_{1u} \leftrightarrow {}^3A_{2g}$	1.262	1.277	1.608	1.623	
	$^3E_u \leftrightarrow {}^3A_{2u}$	−0.000	0.002	0.003	0.011	(0.007[54])
GeV	$^3E_u \leftrightarrow {}^3A_{2g}$	1.595	1.619	2.076	2.105	
	$^3A_{1u} \leftrightarrow {}^3A_{2g}$	1.689	1.726	2.173	2.231	
	$^1E_g \leftrightarrow {}^3A_{2g}$	0.288	0.355	0.329	0.434	
	$^1A_{1g} \leftrightarrow {}^3A_{2g}$	0.529	0.639	0.617	0.797	
	$^1A_{1u} \leftrightarrow {}^3A_{2g}$	1.595	1.621	2.076	2.110	
	$^3E_u \leftrightarrow {}^3A_{2u}$	−0.012	−0.011	−0.012	−0.009	
SnV	$^3E_u \leftrightarrow {}^3A_{2g}$	1.579	1.599	2.069	2.091	
	$^3A_{1u} \leftrightarrow {}^3A_{2g}$	1.667	1.696	2.160	2.207	
	$^1E_g \leftrightarrow {}^3A_{2g}$	0.302	0.368	0.341	0.444	
	$^1A_{1g} \leftrightarrow {}^3A_{2g}$	0.565	0.678	0.649	0.830	
	$^1A_{1u} \leftrightarrow {}^3A_{2g}$	1.570	1.591	2.060	2.086	
	$^3E_u \leftrightarrow {}^3A_{2u}$	−0.017	−0.017	−0.017	−0.014	
PbV	$^3E_u \leftrightarrow {}^3A_{2g}$	1.910	1.934	2.464	2.493	
	$^3A_{1u} \leftrightarrow {}^3A_{2g}$	1.980	2.008	2.533	2.574	
	$^1E_g \leftrightarrow {}^3A_{2g}$	0.321	0.396	0.360	0.476	
	$^1A_{1g} \leftrightarrow {}^3A_{2g}$	0.615	0.750	0.697	0.910	
	$^1A_{1u} \leftrightarrow {}^3A_{2g}$	1.894	1.916	2.446	2.476	
	$^3E_u \leftrightarrow {}^3A_{2u}$	−0.023	−0.024	−0.025	−0.025	

RPA	Beyond-RPA	RPA	Beyond-RPA
39%	33%	1.2%	2.8%
46%	20%	32%	0.67%
110%	1835%	29%	59%
5.1%	4.1%	18%	18%
-	250%	133%	36%

Percent error compared to experiment

Authors state DDH values are in better agreement with the reference values than PBE

Percent error values indicate RPA performs better than beyond-RPA

Excitation Energies

		PBE		DDH		
System	Excitation	RPA	Beyond-RPA	RPA	Beyond-RPA	Ref.
NV	$^3E \leftrightarrow {}^3A_2$	1.395	1.458	1.921	2.001	2.180[7] (1.945[7])
	$^1A_1 \leftrightarrow {}^3A_2$	1.211	1.437	1.376	1.759	
	$^1E \leftrightarrow {}^3A_2$	0.396	0.444	0.476	0.561	
	$^1A_1 \leftrightarrow {}^1E$	0.815	0.993	0.900	1.198	(1.190[8])
	$^3E \leftrightarrow {}^1A_1$	0.184	0.020	0.545	0.243	(0.344–0.430[12])
SiV	$^3E_u \leftrightarrow {}^3A_{2g}$	1.247	1.258	1.590	1.594	1.568[55] (1.31[54])
	$^3A_{1u} \leftrightarrow {}^3A_{2g}$	1.386	1.416	1.741	1.792	
	$^1E_g \leftrightarrow {}^3A_{2g}$	0.232	0.281	0.261	0.336	
	$^1A_{1g} \leftrightarrow {}^3A_{2g}$	0.404	0.478	0.466	0.583	
	$^1A_{1u} \leftrightarrow {}^3A_{2g}$	1.262	1.277	1.608	1.623	
	$^3E_u \leftrightarrow {}^3A_{2u}$	−0.000	0.002	0.003	0.011	(0.007[54])
GeV	$^3E_u \leftrightarrow {}^3A_{2g}$	1.595	1.619	2.076	2.105	
	$^3A_{1u} \leftrightarrow {}^3A_{2g}$	1.689	1.726	2.173	2.231	
	$^1E_g \leftrightarrow {}^3A_{2g}$	0.288	0.355	0.329	0.434	
	$^1A_{1g} \leftrightarrow {}^3A_{2g}$	0.529	0.639	0.617	0.797	
	$^1A_{1u} \leftrightarrow {}^3A_{2g}$	1.595	1.621	2.076	2.110	
	$^3E_u \leftrightarrow {}^3A_{2u}$	−0.012	−0.011	−0.012	−0.009	
SnV	$^3E_u \leftrightarrow {}^3A_{2g}$	1.579	1.599	2.069	2.091	
	$^3A_{1u} \leftrightarrow {}^3A_{2g}$	1.667	1.696	2.160	2.207	
	$^1E_g \leftrightarrow {}^3A_{2g}$	0.302	0.368	0.341	0.444	
	$^1A_{1g} \leftrightarrow {}^3A_{2g}$	0.565	0.678	0.649	0.830	
	$^1A_{1u} \leftrightarrow {}^3A_{2g}$	1.570	1.591	2.060	2.086	
	$^3E_u \leftrightarrow {}^3A_{2u}$	−0.017	−0.017	−0.017	−0.014	
PbV	$^3E_u \leftrightarrow {}^3A_{2g}$	1.910	1.934	2.464	2.493	
	$^3A_{1u} \leftrightarrow {}^3A_{2g}$	1.980	2.008	2.533	2.574	
	$^1E_g \leftrightarrow {}^3A_{2g}$	0.321	0.396	0.360	0.476	
	$^1A_{1g} \leftrightarrow {}^3A_{2g}$	0.615	0.750	0.697	0.910	
	$^1A_{1u} \leftrightarrow {}^3A_{2g}$	1.894	1.916	2.446	2.476	
	$^3E_u \leftrightarrow {}^3A_{2u}$	−0.023	−0.024	−0.025	−0.025	

13 out of 29 (~45%) involve excitations from triplet-to-triplet states, which the authors describe are not significantly affected by the beyond-RPA method

Authors state triplet excitations are insensitive to dielectric screening effects

Intersystem Crossings: finding answers to experimental challenges

SiV struggles experimentally with optical spin polarization

Computational results show $^1A_{1u}$ is higher in energy than the $^3A_{2u} - {}^3E_u$ manifold

Authors suggest this creates energetically unfavorable intersystem crossings

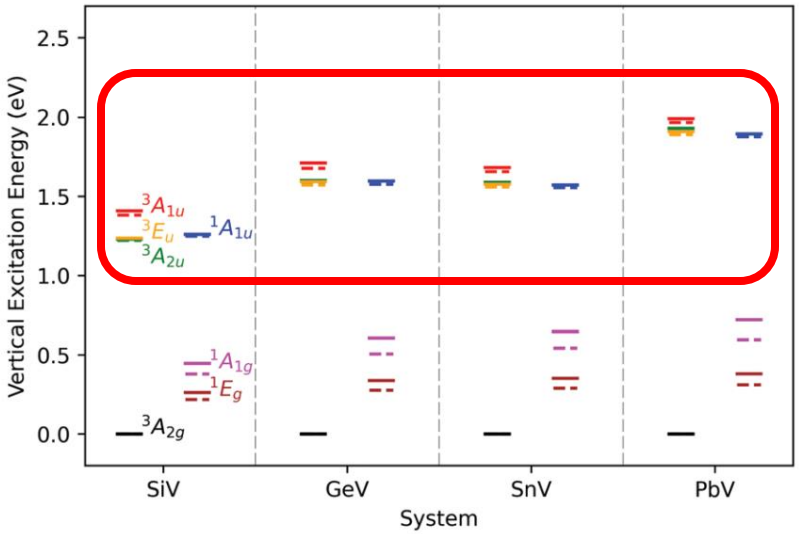

PBE

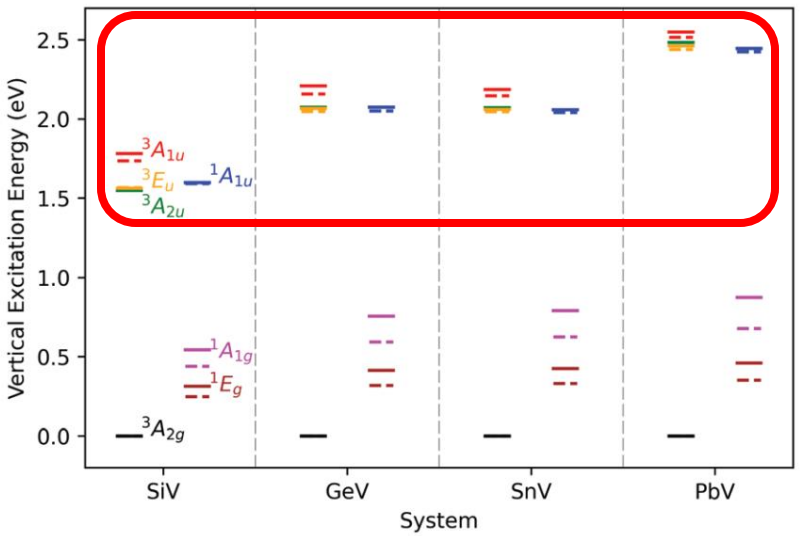

DDH

Conclusions

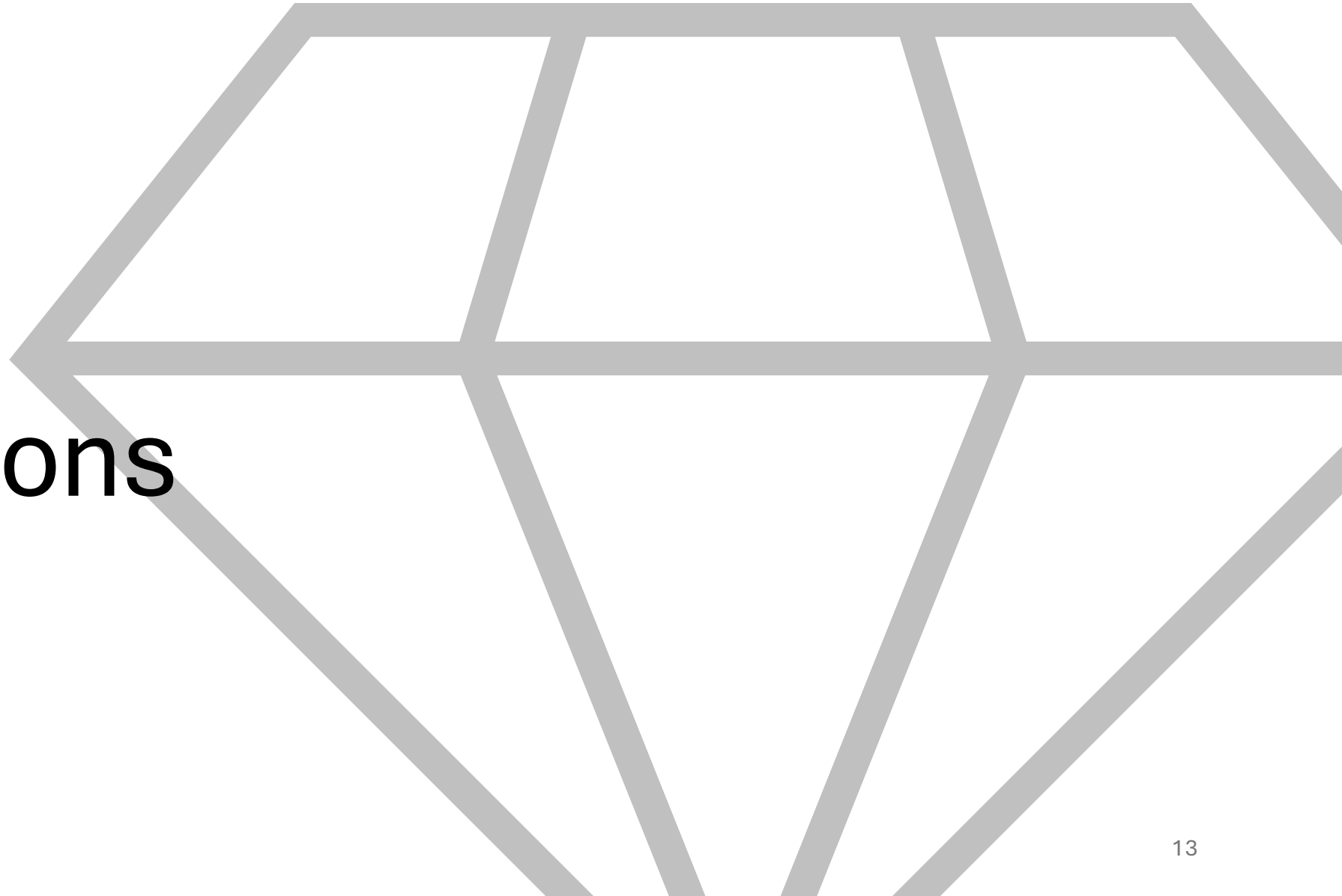

Strengths of the paper

- Provides the first predictions for excited state energies of various diamond-vacancy defects
- Suggests evidence for experimental struggles with optical spin polarization due to intersystem crossings

Weaknesses of the paper

- Little description about the computational theory and method presented
- The beyond-RPA method predicts negative excitation energies for a variety of transitions
- Authors state the inclusion of dielectric screening doesn't affect the excitation energies of triplet states, weakening the main point

Extra Slides

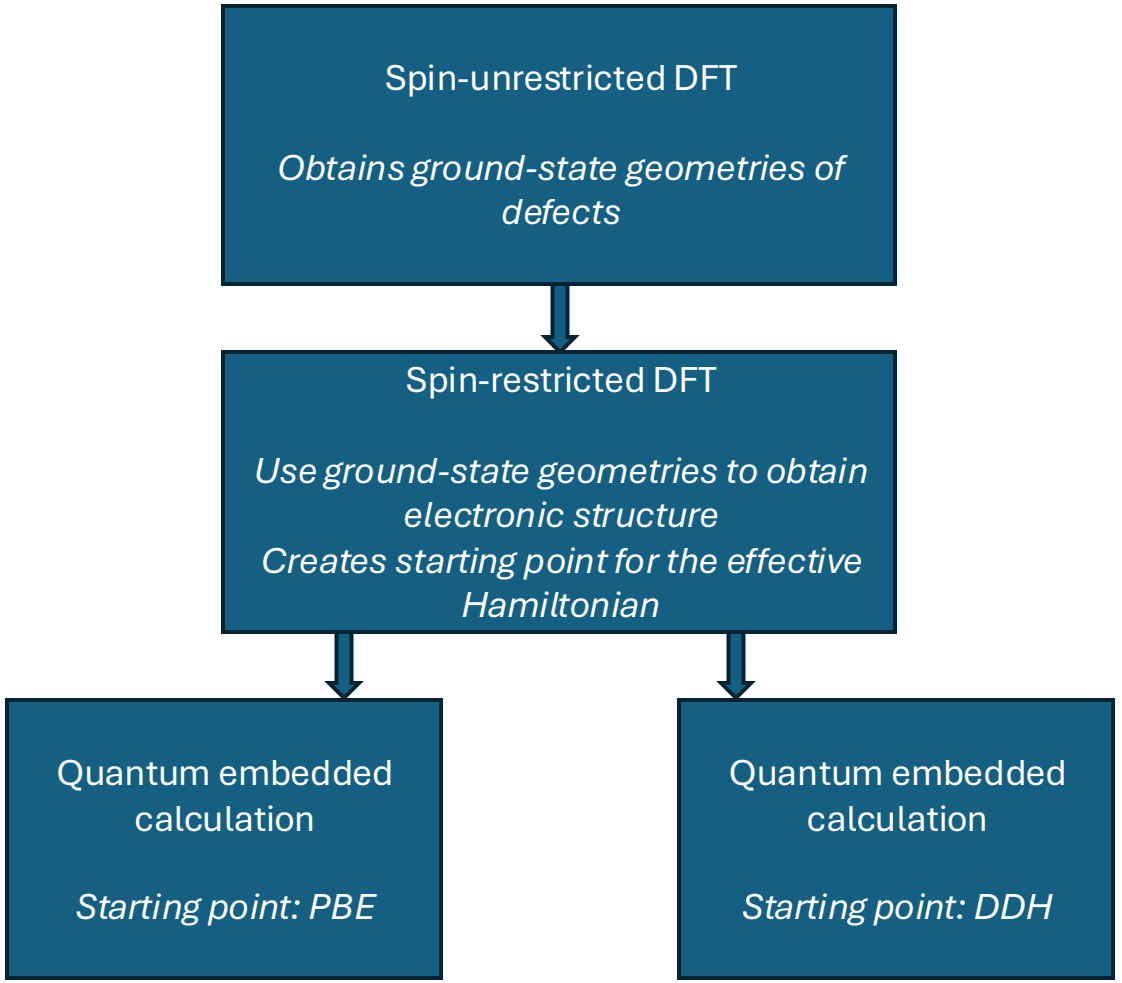
Spin-unrestricted DFT
Obtains ground-state geometries of defects
Spin-restricted DFT
Use ground-state geometries to obtain electronic structure
Creates starting point for the effective Hamiltonian
Quantum embedded calculation
Starting point: PBE
Quantum embedded calculation
Starting point: DDH

Quantum Embedding Theory: going beyond RPA

RPA/cRPA:

$$v^{eff} = v + \chi^{E}_{rpa} v$$

$$\chi^{E}_{rpa} = \chi^{E}_{0} + \chi^{E}_{0} v \chi^{E}_{rpa}$$

χ^{E}_{rpa}
Density response function for the environment, E

Quantum Embedding

$$v^{eff} = v + f X^{E} f$$

$$f = v + f_{xc}$$

f_{xc}
Exchange-correlation kernel
Derivative of the exchange-correlation potential w.r.t. the electron density

Intersystem Crossings: finding answers to experimental challenges

$^1A_{1u}$ is reported slightly higher than the $^3A_{2u} - {}^3E_u$ manifold in the case of SiV, where it is slightly lower for GeV, SnV, and PbV defects. This is suggested to be the reason SiV defects struggle experimentally with optical spin polarization, as the intersystem crossings are energetically unfavored. As the weight of the defect increases, this issue is overcome, and the intersystem crossings are energetically favorable.

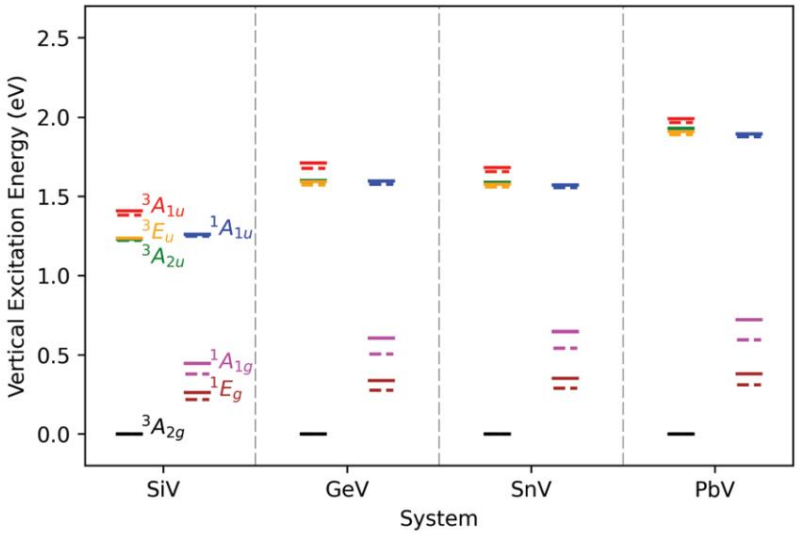

PBE

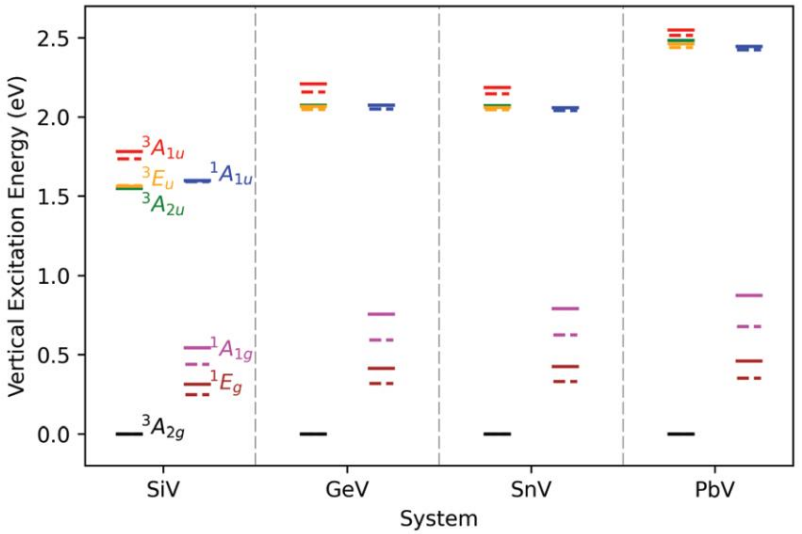

DDH